AIAA 81-1011R

Numerical Experiments on the Leading-Edge Flowfield

Luca Zannetti* and Gino Moretti†
Polytechnic Institute of New York, Farmingdale, New York

A numerical procedure has been developed to analyze the compressible inviscid flowfield in the leading-edge region of an airfoil, using one of the possible variations of the λ scheme: a finite-difference time-dependent method which emphasizes the role of the domain of dependence of each computed point in a transient. The use of artificial permeable boundaries allows the computational domain to be confined to a small region surrounding the nose of the airfoil. A general procedure is described for treating the boundaries without violating the basic principles of the λ scheme and maintaining accuracy at points next to the boundaries.

Nomenclature

a = speed of sound
C = $u+a/\delta$
c,d,e,f = velocities of propagation
D = $u-a/\delta$
E = $v+a/\delta$
F = $v-a/\delta$
l = length
q = flow velocity
R = gas constant
S = entropy
T = temperature
t = time
u,v = Cartesian velocity components
x,y = Cartesian coordinates
z = complex variable on the physical plane
γ = ratio of specific heats
δ = $(\gamma-1)/2$
ρ,θ = polar coordinates
ζ = complex variable on the computational plane

All quantities are normalized with respect to reference values:

$$l_{\text{ref}},\ T_{\text{ref}},\ S_{\text{ref}},\ q_{\text{ref}}=(RT_{\text{ref}})^{1/2},\ t_{\text{ref}}=l_{\text{ref}}/q_{\text{ref}}$$

Introduction

THE main purpose of this paper is to show the capabilities of a numerical technique that is strongly based on physical concepts. Such a technique is time dependent and can be applied to mixed initial- and boundary-value problems of unsteady, inviscid, compressible flows.

The flowfield on the leading edge of an airfoil has been chosen as a test example. Such a flowfield has some difficult features because of the presence of a stagnation point and of the strong, generally transonic, expansion around a nose having a small radius of curvature. Moreover, the flowfield has been computed only within a small region around the leading edge in such a way that the flow across any nonrigid, artificial boundary is subsonic. The region is shown in Fig. 1, where AB is the rigid wall of the airfoil nose, CD an inlet permeable surface, and BC, DA exit permeable surfaces. Such permeable boundaries are treated following the main guidelines of Refs. 1-3. Briefly, they act as actuator disks which prescribe the flow angles on their downstream side; across such disks, quasisteady relations of conservation of mass flow, total enthalpy, and entropy hold.

So far, this kind of boundary has been used mostly to solve problems of internal gasdynamics. Here, an application to external flow problems is presented. When the overall Mach numbers are very low, an asymptotically steady solution can be reached, compatible with a given uniform flow at infinity, by prescribing boundary values consistent with the incompressible, potential flow about the same body. If compressibility effects are sizeable, it is not possible to relate the values prescribed at the boundaries to any condition at infinity prescribed a priori. Nevertheless, the qualitative picture of the flowfield around an airfoil leading edge is maintained and a large variety of flows can be simulated, including cases where the total pressure and/or the total temperature are not uniform, as it happens for an airfoil inside a wake or a jet plume.

Thus, it is clear that the present problem is affected by many of the difficulties which currently appear in numerical calculations: strong gradients, transonic flow, stagnation points, and artificial subsonic boundaries in regions strongly perturbed by the body, where the far field conditions are of little relevance. Therefore, we consider this problem to be well suited for a test of a numerical technique as a whole, as well as of each of its details.

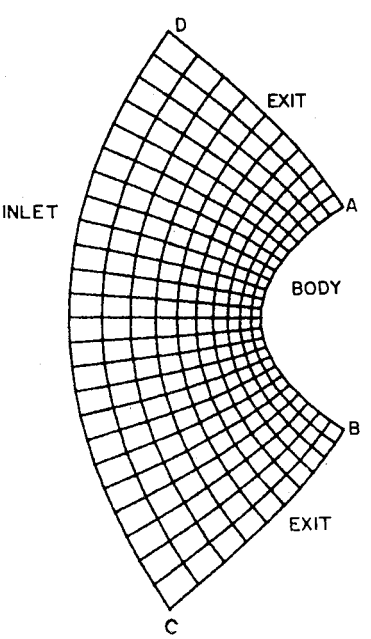

Fig. 1 Computational grid around leading edge.

Presented as Paper 81-1011 at the AIAA Fifth Computational Fluid Dynamics Conference, Palo Alto, Calif., June 22-23, 1981; submitted June 29, 1981; revision received March 3, 1982.

*Research Associate; presently Associate Professor, Politecnico di Torino.
†Professor. Fellow AIAA.

Numerical Technique

The finite difference method which we use is a version of the λ scheme, based on the ideas expressed several years ago in Ref. 4 and, more recently, in Ref. 5. The present version was introduced in Ref. 6. The general philosophy of the method is based on the observation that the Euler equations for unsteady flow essentially describe a phenomenon of wave propagation. According to Levi-Civita,[7] the very peculiar aspect that characterizes wave propagation phenomena is the discontinuity of the derivatives of a certain order. In fact, something can be said to propagate if it is possible to find a wave front that separates the region as yet unperturbed from the perturbed one. Across such a wave front, generally, a discontinuity is to be found. This statement is the well-known physical interpretation of the mathematical concepts of domain of dependence and characteristic variety. When a hyperbolic system of equations has to be solved numerically, the discretized technique should save as many as possible of the physical properties which the partial-differential equations imply.

The λ scheme is based on the idea that the space derivatives can be discontinuous. Consequently, the information used to approximate them must be taken from points that lie as close as possible to the domain of dependence. In Ref. 6 it is shown how the governing equations can be recast as suitable combinations of compatibility relations on characteristic surfaces. The local time derivatives of the flow appear to depend only on the space components of derivatives along bicharacteristics. The space derivatives, in turn, are approximated by one-sided differences, according to the direction of propagation along the bicharacteristics. Therefore, the evolution of the flow in time is approximated as the effect of a discrete system of wave fronts converging upon each mesh point at each time step. As many waves are needed as sufficient to eliminate, by linear combinations, space derivatives not related to bicharacteristics. Similar ideas are expressed by Butler[8] with reference to a method of characteristics. Four bicharacteristics and the streamline are needed in the two-dimensional case; six bicharacteristics and the streamline in the three-dimensional case.

In Ref. 6 it is also suggested that the space derivatives be performed on certain combinations of the flow primitive variables which can be interpreted as multi-dimensional generalizations of the Riemann invariants of the one-dimensional flow. By so doing, specific variables are related to each bicharacteristic. These variables express the information carried by each wave front, strengthening the physical meaning of the method. Moreover, such variables exploit the capability of "capturing" shock waves which the λ scheme shows in many cases.

To extend the analysis of Ref. 6 to a more general, nonhomoentropic flowfield, we proceed as follows. At a point where the flow is subsonic, the system of four bicharacteristics and the streamline converging on a mesh point appear as in Fig. 2a, where vectors representing the velocity of a particle (q) and the velocities of propagation of signals along each characteristic (c, d, e, f) are shown. The pattern for a supersonic case is shown in Fig. 2b. For brevity, we use the notations

$$C' = (u+a)(C_x - \kappa S_x)^c, \qquad D' = (u-a)(D_x + \kappa S_x)^d$$

$$E' = (v+a)(E_y - \kappa S_y)^e, \qquad F' = (v-a)(F_y + \kappa S_y)^f$$

with $\delta = (\gamma-1)/2$ and $\kappa = a/2\gamma\delta$. The superscripts (c, d, e, f and in the following, q) denote to which bicharacteristic in Fig. 2 the space derivatives are related. For instance, the derivatives C_x^c, C_y^c, and S_x^c are related to the bicharacteristic whose velocity of propagation is c; therefore, according to Fig. 2a, they have to be evaluated by differences on the sides of the third quadrant. Using the preceding notations, the

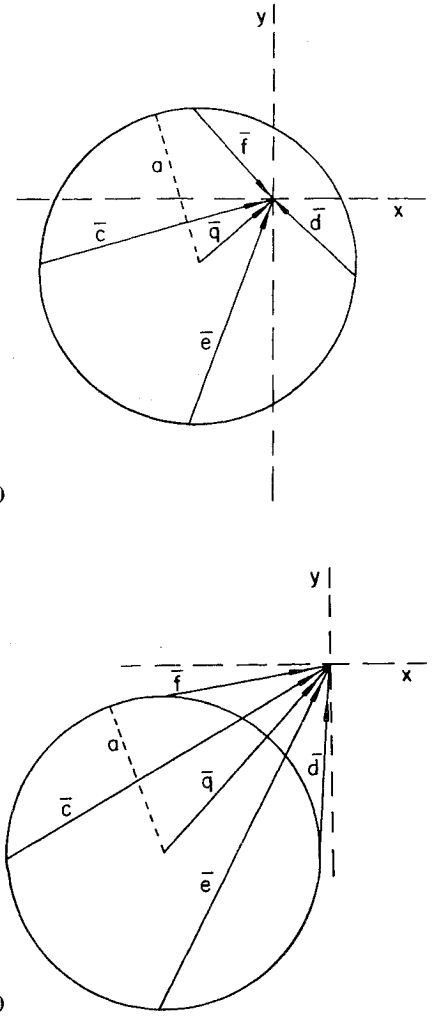

Fig. 2 Traces of Mach cones and bicharacteristics.

equations of motion for a two-dimensional flow, in Cartesian coordinates, are

$$S_t = -uS_x^q - vS_y^q \qquad a_t = -\frac{\delta}{2}[C' - D' + E' - F'] + \kappa\delta S_t$$

$$u_t = -\frac{1}{2}[C' + D' + v(C_y^c + D_y^d)]$$

$$v_t = -\frac{1}{2}[u(E_x^e + F_x^f) + E' + F'] \qquad (1)$$

The extension to three-dimensional flows, as well as to a more general system of coordinates, is direct and it is given in Ref. 6 for the homoentropic case.

Numerical Schemes

The integration scheme used to perform the present numerical experiments has been devised by Gabutti[9] for the λ scheme. It is a second-order, two-level scheme; it has some advantages in comparison with the original λ scheme of Ref. 5 since the number of points needed, in each direction, equals three instead of four. The present analysis, however, is valid for both algorithms.

A large number of variations on the λ scheme has appeared recently, as well as a number of schemes, mostly related to an original formulation of Euler's equations in conservation form. In many cases, different schemes become identical for linear problems. In nonlinear cases, some schemes prove to be

more efficient, or easier to apply than others. The techniques are still in a phase of development, and it is hard to recommend any one of them in particular. The reader must be warned, however, against confusion. For example, it has been said that Gabutti's scheme is the same as Warming and Beam's.[10] This is not true for nonlinear problems. In all λ schemes, a weighted contribution from the upstream and downstream domains of dependence is automatically taken in subsonic flows, in this way assuring a smooth transition to supersonic domains, where the contributions are from upstream only. Warming uses a hybrid combination of centered differences for subsonic flows and upwind differences for supersonic regions. Other interesting properties of the λ schemes[9] are their low numerical viscosity and the presence of a fourth-order dissipation term which gives such schemes strong shock-capturing powers.

In the present work, the scheme is applied as follows. Let us consider a general, quasi-linear equation,

$$g_t + \lambda g_x = 0 \tag{2}$$

where $\lambda = \lambda(g)$ is the slope of the characteristic on the (x,t) plane. In the case $\lambda > 0$, the integration scheme can be written as follows.

Predictor

$$\tilde{g}_i^{n+1} = g_i^n - \lambda g_x \Delta t$$

where

$$g_x = (g_i^n - g_{i-1}^n)/\Delta x$$

Corrector

$$g_i^{n+1} = g_i^n - \tilde{\lambda}(\tilde{g}_x + \hat{g}_x)(\Delta t/2)$$

where

$$\tilde{g}_x = (\tilde{g}_i^{n+1} - \tilde{g}_{i-1}^{n+1})/\Delta x$$

$$\hat{g}_x = 2\frac{g_i^n - g_{i-1}^n}{\Delta x} - \frac{g_{i-1}^n - g_{i-2}^n}{\Delta x} \tag{3}$$

In the corrector level, the scheme uses a three-point formula, Eq. (3). In a mixed initial- and boundary-value problem, application of the formula is not straightforward at point $i=2$ next to the boundary, for which three points are not available. The difficulty can be overcome in many different ways. For instance, a suitable extrapolation from inner points could be used to compute the extra point beyond the boundary, still maintaining second-order accuracy. The procedure, however, would involve at least point $i=3$, and it would be inconsistent with the general principle of strict abidance by the domain of dependence, which we have decided to adopt. We prefer to modify the scheme at the points next to the boundaries, in such a way that the points are still chosen on the same side prescribed for the two-point formula by the domain of dependence, and the second-order accuracy is maintained. The formula, again, is based on physical considerations. In Eq. (2), the derivative g_x is the space component of the derivative along the characteristic which brings signals from the boundary to the interior region; therefore, an algorithm at point $i=2$, which calls for information from a region as wide as two mesh intervals, must use the boundary condition explicitly in order to provide for the interval to the left of the boundary, which is missing. Looking at how the scheme works at a general interior point, it is natural to modify Eq. (3) at point $i=2$ in the following way.

$$\hat{g}_x = 2[(g_2^n - g_1^n)/\Delta x] - g_x^b \tag{4}$$

where g_x^b is computed at the boundary point $i=1$, at the predictor level by

$$g_x^b = -g_t/\lambda$$

and g_t is provided by the boundary condition.

Computation at the Boundaries

The general philosophy followed here for the computation of boundary points has been expressed in Ref. 11. The flow properties at the boundaries are computed by matching the boundary conditions with compatibility relations which describe signals impinging on the boundaries from interior points. That is, indeed, a very natural procedure for the λ scheme, and physically correct.

The computation at the boundaries has been organized here in a way quite simple to be coded, well in harmony with the computation of interior points. By considering how the interior points are computed, it turns out that at the boundaries a certain number of terms of Eqs. (1), that is, the ones which bring information from outside, cannot be evaluated and become additional unknowns. The number of boundary conditions at a boundary, however, is the same as the number

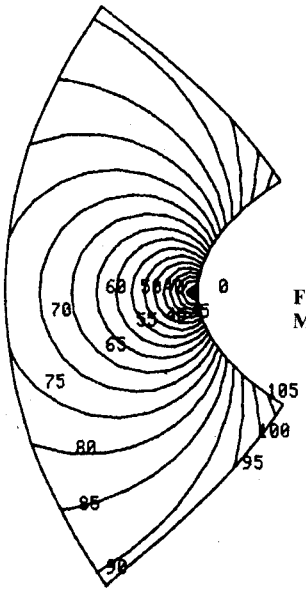

Fig. 3 Thick ellipse, initial Mach lines.

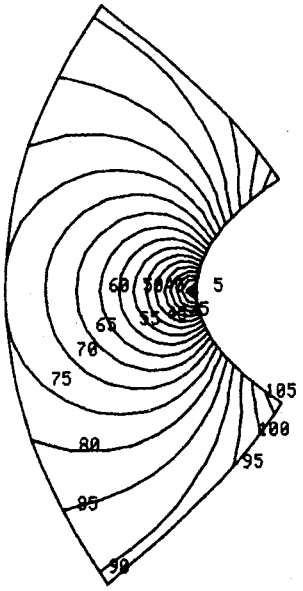

Fig. 4 Thick ellipse, computed, steady Mach lines.

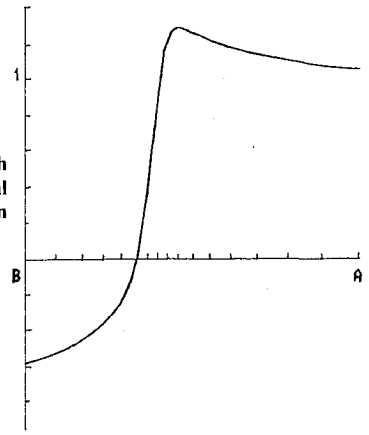

Fig. 5 Slender ellipse with supersonic outflow; initial Mach number distribution along the body.

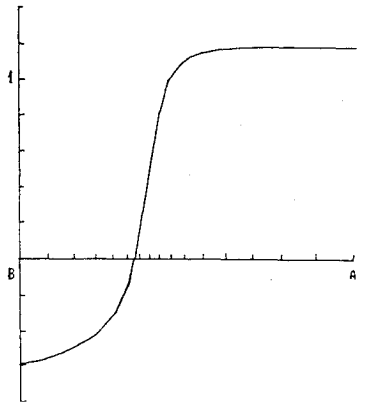

Fig. 6 Slender ellipse with supersonic outflow; computed, steady Mach number distribution along the body.

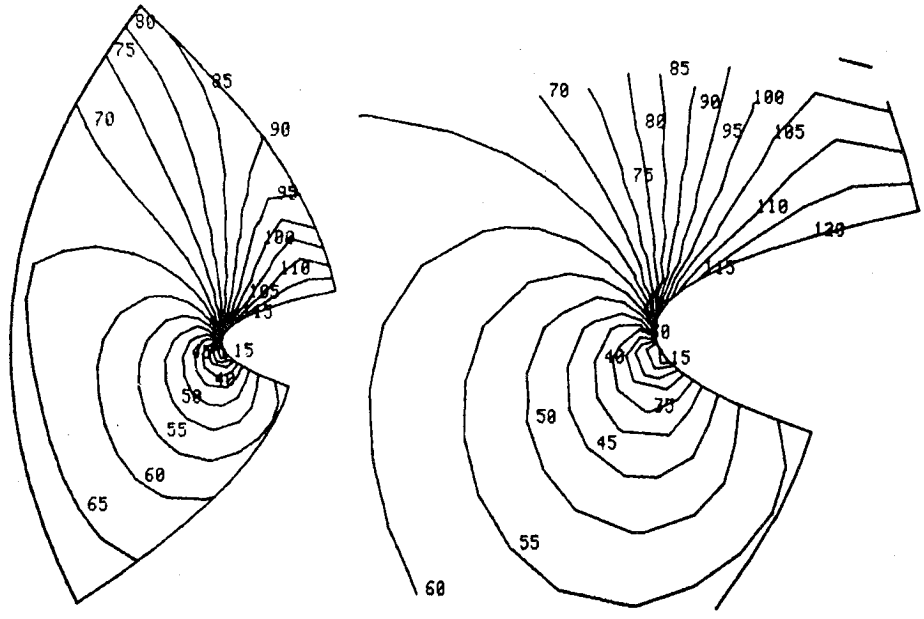

Fig. 7 Slender ellipse with supersonic outflow; computed Mach lines.

of such unknowns. Consequently, the problem can be solved. For instance, let us suppose that the y-coordinate line of Fig. 2a is an inlet permeable boundary (with the computational region to the right of it). According to the domains of dependence, $(C_x-\kappa S_x)^c$, $E_x^e+F_x^f$, and S_x^q cannot be computed. There are, instead, three boundary conditions at this boundary; in the present examples, we assume the total temperature T_0, the entropy S, and the slope of the streamline v/u as known. The terms $(C_x-\kappa S_x)^c$, $E_x^e+F_x^f$, and S_x^q, so obtained, allow the boundaries to be computed using the same equations and the same algorithm as at interior points. Moreover, such terms are precisely the terms needed at the point next to the boundary, according to Eq. (4) and neglecting the slight nonlinearity of $(C_x-\kappa S_x)^c$.

In a similar manner, let us suppose now that the y-coordinate line of Fig. 2a is an exit permeable boundary (with the computational region to the left of it). There is only one unknown term in this case, the term $(D_x+\kappa S_x)^d$, and the boundary condition has to be one relation between the flow properties at the exit. In the present examples the flow Mach number is prescribed, as a particular variation of the boundary condition discussed in Ref. 2.

Finally, let us suppose now that the y-coordinate line is a solid wall and the flowfield is on the positive side of the x axis. The boundary condition is now the vanishing of the velocity component normal to the wall, $u=0$, so that the only unknown term is $(C_x-\kappa S_x)^c$.

Numerical Experiments

Arcs of ellipses have been chosen to simulate noses of airfoils. The outside of the ellipse in the physical plane, $z=x+iy$, is mapped onto the inside of the unit circle in the computational plane, $\zeta=\rho\exp(i\theta)$, using the Joukowski mapping: $z=\zeta+1/\zeta$. The circles, $\rho+\text{const}$ $(\rho<1)$, of the ζ plane are mapped onto ellipses on the z plane. The closer the radius ρ to 1 is, the slenderer the ellipse. By using a polar frame of reference on the ζ plane, the computational domain is defined by selecting the radius, ρ_b of the circular arc, image of the body; the radius ρ_i of the circular arc, image of the inlet permeable surface; and the angles θ_A, θ_B of the straight segments, images of exit permeable surfaces.

The first example refers to a domain defined by $\rho_b=0.75$, $\rho_i=0.5$, $\theta_A=198$ deg, and $\theta_B=166$ deg. At the inlet boundary the boundary conditions are chosen as follows. First, the entropy at inlet points is set equal to zero, and the total temperature is assumed to be uniform, with a value consistent with a Mach number at infinity M_∞ equal to 0.1. Then, the incompressible, potential flow at no incidence ($\alpha=0$ deg) is determined. The corresponding slopes of the streamlines at inlet points are accepted as valid for the current calculation. A Mach number distribution is prescribed at exit points, consistent with the total temperature above and the velocity distribution of the incompressible flow. Similarly, an initial flow configuration is guessed, taking the velocity vectors from the incompressible flow; Mach number and pressure are

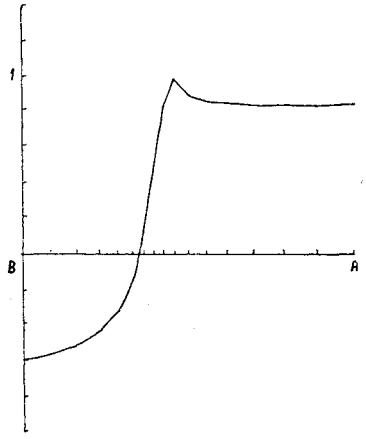

Fig. 8 Slender ellipse with subsonic outflow; initial Mach number distribution along the body.

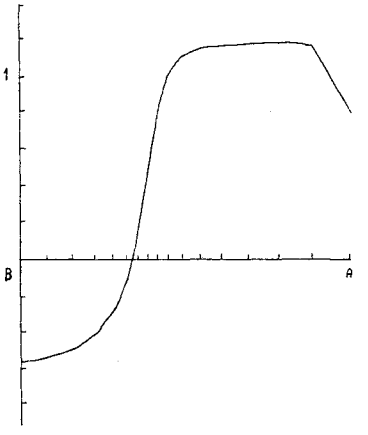

Fig. 9 Slender ellipse with subsonic outflow; computed, steady Mach number distribution along the body.

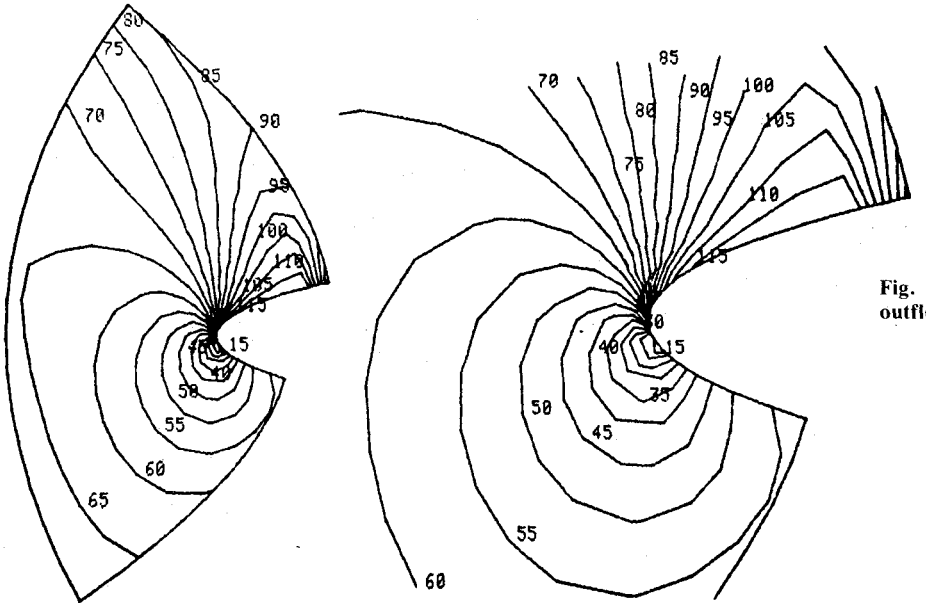

Fig. 10 Slender ellipse with subsonic outflow; computed Mach lines.

evaluated as consistent with the assumed total temperature and constant entropy. The initial Mach number distribution is shown in Fig. 3. Because of the low Mach number range, the initial flow configuration can be assumed as a good approximation of the compressible steady solution. The steady computed Mach number distribution, after 500 time steps, is shown in Fig. 4. The agreement between Figs. 3 and 4 is remarkable; the points next to the boundaries look in smooth alignment with boundary and interior points.

The second example refers to a more slender ellipse. The geometrical parameters of the computational domain are now $\rho_b = 0.93$, $\rho_i = 0.65$, $\theta_A = 198$ deg, $\theta_B = 166$ deg. The values prescribed at the boundaries and the initial flow configuration are again based on the incompressible solution for potential flow and for an incidence $\alpha = 2$ deg, but now the total temperature is set as consistent with the Mach number at infinity, $M_\infty = 0.8$. The initial configuration is now very dissimilar from the steady solution. The flow is transonic. A portion of the exit surface on the upper side is guessed as supersonic; the flow on it does not depend on downstream conditions and, therefore, boundary conditions do not have to be provided for it. This is quite a delicate situation for the exit boundary, which cuts across a supersonic bubble and only partially acts as an artificial subsonic permeable boundary.

The initial Mach number distribution along the body is shown in Fig. 5, while Fig. 6 shows the computed steady distribution. Figure 7 shows lines of constant Mach number on the computed flowfield and an enlarged view of the region surrounding the body, with the supersonic bubble cut through by the exit surface on the upper side.

As formerly stated, such a flowfield cannot be related to any condition at infinity, in which all physical parameters are prescribed a priori. It shows, however, that suitable models can be defined in order to perform a local analysis of the region of the stagnation point and of the strong expansion around the leading edge. We believe that the analysis would be hard to perform if other models for the treatment of subsonic boundaries were used, and that in most attempts catastrophic instabilities would appear.

The last example refers to the following numerical experiment. The initial flow configuration and the boundary conditions are obtained by the steady flow configuration as computed on the previous example, but all the supersonic values are replaced by the corresponding subsonic values obtained by assuming the same total temperature, the same entropy, and the same mass flow. The initial flowfield is now fully subsonic and, again, far from a steady solution. The exit upper boundary is now subsonic; as stipulated earlier, the Mach number initially computed along it is kept constant in time. As a result of these boundary conditions, the mass flow across the exit boundary will be the same as in the previous example, when a steady state is reached. Therefore, we expect to obtain a flow pattern very similar to the one of Fig. 7, except for the appearance of a jump, necessary to close the

supersonic bubble before it reaches the exit boundary. That such a change actually occurs is shown by Figs. 8-10. Figure 8 shows the initial distribution of Mach numbers along the body and Fig. 9 shows the steady Mach number distribution along the body, as computed. Figure 10 presents the computed flowfield (isomachs).

In this case, as well as in other cases described in Refs. 5 and 6, the λ scheme shows its remarkable capability to describe jumps as sharp transitions across a single mesh interval, without generating spurious numerical oscillations.

References

[1] Pandolfi, M., "Transonic Swirling Flow in Axisymmetric Nozzles," *Meccanica,* Vol. 11, No. 3, 1976, pp. 157-161.

[2] Pandolfi, M. and Zannetti, L., "Some Permeable Boundaries in Multidimensional Flows," 6th International Conference on Numerical Methods in Fluid Dynamics, Tbilisi, June 1978, pp. 439-446.

[3] Moretti, G. and Pandolfi, M., "Critical Study of Calculations of Subsonic Flows in Ducts," *AIAA Journal,* Vol. 19, April 1981, pp. 449-457.

[4] Courant, R., Isaacson, E., and Rees, M., "On the Solution of Nonlinear Hyperbolic Differential Equations by Finite Differences," *Communications on Pure and Applied Mathematics,* Vol. 5, 1952, pp. 243-255.

[5] Moretti, G., "The λ-scheme," *Computers and Fluids,* Vol. 7, 1979, p. 191.

[6] Zannetti, L. and Colasurdo, G., "Unsteady Compressible Flow: A Computational Method Consistent with the Physical Phenomena," *AIAA Journal,* Vol. 19, July 1981, pp. 852-856.

[7] Levi-Civita, T., *Caratteristiche dei Sistemi Differenziali e Propagazione Ondosa,"* Zanichelli, 1931, pp. 21 and 42.

[8] Butler, D. S., "The Numerical Solution of Hyperbolic Systems of Partial Differential Equations in Three Independent Variables," *Proceedings of the Royal Society,* Series A, 1960, Vol. 255, pp. 232-252.

[9] Gabutti, B., "On Two Upwind Finite-Difference Schemes for Hyperbolic Equations in Non-Conservative Form," to appear in *Computers and Fluids.*

[10] Warming, R. F. and Beam, R. M., "Upwind Second-Order Difference Schemes and Applications in Aerodynamic Flows," *AIAA Journal,* Vol. 14, Sept. 1976, pp. 1241-1249.

[11] Moretti, G., "Importance of Boundary Conditions in the Numerical Treatment of Hyperbolic Equations," *Physics of Fluids,* Vol. 12, 1969, p. 12.